NASA
Technical Memorandum 107388

Army Research Laboratory
Technical Report ARL–TR–1252

Three-Dimensional Flow Field Measurements in a Transonic Turbine Cascade

P.W. Giel
NYMA, Inc.
Brook Park, Ohio

D.R. Thurman and I. Lopez
U.S. Army Research Laboratory
Lewis Research Center
Cleveland, Ohio

R.J. Boyle, G.J. Van Fossen, T.A. Jett,
W.P. Camperchioli, and H. La
Lewis Research Center
Cleveland, Ohio

Prepared for the
41st Gas Turbine and Aeroengine Congress
sponsored by the International Gas Turbine Institute of
the American Society of Mechanical Engineers
Birmingham, United Kingdom, June 10–13, 1996

National Aeronautics and
Space Administration

THREE-DIMENSIONAL FLOW FIELD MEASUREMENTS IN A TRANSONIC TURBINE CASCADE

P. W. Giel
NYMA, Inc.
Engineering Services Division
Brook Park, OH

D. R. Thurman, I. Lopez
U.S. Army Research Laboratory
NASA Lewis Research Center
Cleveland, OH

R. J. Boyle, G. J. Van Fossen,
T. A. Jett, W. P. Camperchioli, and H. La
NASA Lewis Research Center
Cleveland, OH

ABSTRACT

Three-dimensional flow field measurements are presented for a large scale transonic turbine blade cascade. Flow field total pressures and pitch and yaw flow angles were measured at an inlet Reynolds number of 1.0×10^6 and at an isentropic exit Mach number of 1.3 in a low turbulence environment. Flow field data was obtained on five pitchwise/spanwise measurement planes, two upstream and three downstream of the cascade, each covering three blade pitches. Three-hole boundary layer probes and five-hole pitch/yaw probes were used to obtain data at over 1200 locations in each of the measurement planes. Blade and endwall static pressures were also measured at an inlet Reynolds number of 0.5×10^6 and at an isentropic exit Mach number of 1.0. Tests were conducted in a linear cascade at the NASA Lewis Transonic Turbine Blade Cascade Facility. The test article was a turbine rotor with 136° of turning and an axial chord of 12.7 cm. The flow field in the cascade is highly three-dimensional as a result of thick boundary layers at the test section inlet and because of the high degree of flow turning. The large scale allowed for very detailed measurements of both flow field and surface phenomena. The intent of the work is to provide benchmark quality data for CFD code and model verification.

LIST OF SYMBOLS

C_x	-	blade axial chord [cm]
M	-	Mach number
p	-	blade pitch [cm]
P	-	pressure [Pa]
Re_{C_x}	-	Reynolds number, $Re = \rho U_{in} C_x / \mu$
s	-	blade span [cm]
Tu	-	turbulence intensity
U	-	total velocity [m/s]
x	-	chordwise (axial) direction
y	-	pitchwise (tangential) direction
z	-	spanwise (radial) direction
α	-	pitch angle (x–y plane) [degrees]
β	-	yaw angle (x–z plane) [degrees]
μ	-	dynamic viscosity [kg/s·m]
ρ	-	density [kg/m^3]
δ	-	boundary layer thickness [cm]
τ	-	probe time constant [seconds]
Subscripts		
ex	-	exit freestream value
f	-	full (99%) boundary layer thickness
in	-	inlet freestream value
IS	-	isentropic value
o	-	average of outer probe ports
1 - 5	-	probe ports
Superscripts		
$'$	-	total conditions

INTRODUCTION

There is a continuing need to provide benchmark quality experimental data for the verification of turbomachinery CFD analyses. Improvements in computational speeds and storage availability allow CFD analyses to resolve the flow features in increasingly greater detail. To verify the computational analyses, as well as to provide data for improved modeling of the flow features, experiments which resolve the flow field in fine detail are needed. To help satisfy this need, a Transonic Turbine Blade Cascade was designed and built at the NASA-Lewis Research Center. The purpose of this facility is to obtain detailed aerodynamic and heat transfer measurements for turbomachinery blading that is characteristic of advanced turbomachinery applications. The facility is configured to provide detailed aerodynamic and heat transfer data for engine-relevant geometries, Reynolds numbers, and Mach numbers. This facility is a linear cascade. It was recognized that a linear cascade cannot simulate rotation effects, and that the chosen design does not allow for tip clearance effects. Nonetheless, a linear cascade was chosen over an annular cascade for a number of reasons. The primary reason was to obtain detailed measurements in a large scale facility at transonic flow conditions. The physical size of the blading was determined by the amount of air that could be moved at transonic speed through the cascade. An annular cascade of engine-typical hub-to-shroud and aspect ratios would require several times more flow rate than a linear cascade for blades of the same chord length. Also, a linear cascade provides easier access for instrumentation than an annular cascade. From a computational aspect, a linear geometry minimizes the effects of the three-dimensional mesh on the CFD solution, thus giving a clearer analysis of the actual flow solver. The initial configuration for the cascade is a rotor geometry.

Several researchers have reported results of aerodynamic measurements for rotor geometries tested in linear cascades. Graham and Kost (1979) showed results for two turbine rotor geometries tested at transonic conditions. Kiock et al. (1986) evaluated the differences in rotor performance seen when the same rotor geometry was tested in four different wind tunnels at transonic conditions. Mee et al. (1992a) and Mee et al. (1992b) presented measurements for a rotor linear cascade tested at transonic conditions in a short duration blowdown facility. Mee et al. (1992a) focuses on the measurement of midspan loss mechanisms while Mee et al. (1992b) focuses on detailed blade boundary layer measurements, primarily at midspan. In addition to measurements made at transonic flow conditions, several researchers presented results for rotor geometries tested in low speed linear cascades. Generally, these results were obtained in cascades with blading significantly larger than that used in the transonic tests. Langston et al. (1977), Gregory-Smith and Graves (1983), Marchal and Sieverding (1977), Yamamoto (1987a,b), Moustapha et al. (1985), and Gregory-Smith et al. (1988) presented detailed results of aerodynamic measurements for rotor blades tested in linear cascades at relatively low Mach numbers.

The test configuration for the present study was a linear cascade of ten whole blades and two shaped end-blades, giving eleven passages. Each blade had an axial chord of 12.7 cm (5.00 in.). The facility was designed to have a maximum test section total pressure of approximately one atmosphere. Transonic flow conditions were achieved by passing the air from the test section to a low pressure exhaust system. The combination of low total pressures and large-size blading allows the facility to simulate engine-relevant Reynolds and Mach numbers using test geometries significantly larger than found in actual engines.

The blade tested in the cascade is of constant cross section so that the geometry of the cascade is two-dimensional. Verification data for three-dimensional CFD analyses was desired. The three dimensionality of the flow field was achieved by not bleeding off the endwall boundary layers. It will be shown that, when the endwall boundary layers are not bled off, the spanwise variation of surface pressures around the rotor was of the same order as the spanwise variation in surface pressures experienced in an actual engine.

The objective of the work presented in this paper was to obtain aerodynamic measurement data. The data was intended to be of benchmark quality and to be of sufficient detail so as to be useful for validating CFD analyses. Measurements presented here include blade and endwall static pressures, flow-field measurements of total pressure, along with pitch and yaw flow angles. Pitchwise integrated averages of all of these quantities will be presented as well. Flow field measurements were made on two survey planes upstream and three survey planes downstream of the blade row. All of the flow-field measurements were obtained with either a 3-hole boundary-layer probe or a 5-hole pitch/yaw probe. A description of the probes that were used and their calibrations are also included. The aerodynamic measurements described here are intended to complement the endwall heat transfer measurements that were made in the same facility and described by Giel et al. (1996).

All of the flow field data presented here was obtained at a nominal inlet Reynolds number of 1.0×10^6 and at a nominal exit Mach number of 1.3. Blade and endwall static pressure data were also obtained at a Reynolds number of of 0.5×10^6 and at an exit Mach number of 1.0. Upstream of the blade row, the inlet freestream turbulence intensity level was approximately 0.25%.

DESCRIPTION OF FACILITY

An initial description of the facility was given by Verhoff et al. (1992). Since that time, an inlet section analysis and redesign (Giel et al., 1994) was performed to improve inlet flow pitchwise uniformity. Figure 1 shows an overall view of the facility with the new inlet section in place. High pressure air at ambient temperature is supplied to the facility. The air is throttled to a maximum pressure of 120 kPa (17 psia) in the test section. The air passes through the blade row and is then discharged into an exhaust header maintained at a nominal pressure of 15.9 kPa (2.3 psia). Valves between the test section and the exhaust header are adjusted to give the desired static-to-inlet total pressure ratio at the blade row exit. As seen in Fig. 1, the test section is mounted on a large disk. This disk can be rotated to give a range of incidences. All of the results described here were obtained at the design inlet flow angle of 63.6 degrees. This inlet angle gave a flow turning of about 136 degrees. Upstream inlet boards were installed as described in Giel et al. (1994), but to prevent shock reflections in the downstream section, no exit tailboards were used. A highly three-dimensional flow field was obtained in the blade passages by allowing boundary layers to develop in the long inlet section upstream of the cascade. Aerodynamic probe data and blade loading data both verify the existence of strongly three-dimensional passage flow.

The blade shape used in these tests, while generic in nature, was designed to simulate the flow characteristics of a high specific work rotor. Pertinent details of the blade and of the cascade are given in Table 1. A detailed view of the test section is shown in Fig. 2. The figure shows the two upstream measurement planes (Stations 0 and 1) and the three downstream measurement planes (Stations 2, 3, and 4). These measurement planes extend from the endwall, $z = 0$, to just above midspan, $z/s = 0.54$. Each of the passages is numbered in the figure, and Passage 5 was considered to be the primary test passage.

Inlet freestream turbulence intensity measurements were made with a constant-temperature hot wire anemometer traversed in Station 0 ($x/C_x = -1.000$, see Fig. 2). The measurements showed a pitchwise uniform freestream value of Tu equal to 0.25% at $Re_{C_x} = 1.0 \times 10^6$ and 0.50% at $Re_{C_x} = 0.5 \times 10^6$.

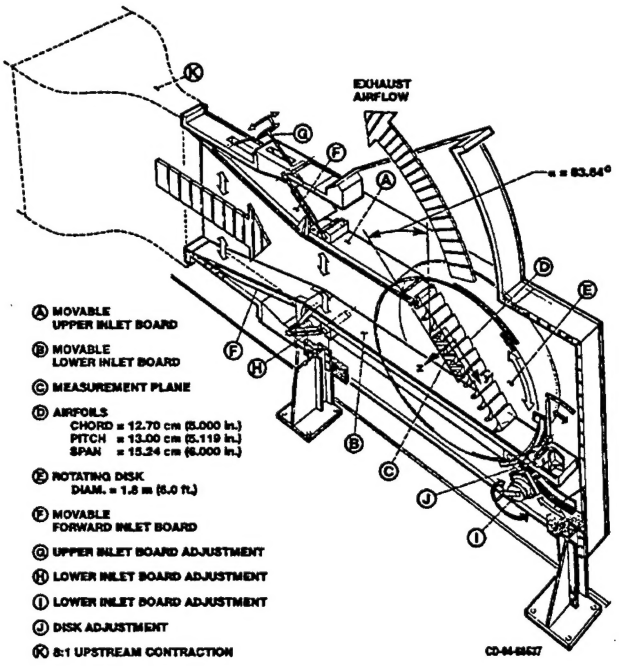

Fig. 1 Overall view of Transonic Turbine Blade Cascade test section

Table 1 Blade and cascade parameters and dimensions

Geometric parameter	Value
axial chord	12.70 cm (5.000 inches)
pitch	13.00 cm (5.119 inches)
span	15.24 cm (6.000 inches)
true chord	18.42 cm (7.250 inches)
stagger angle	41.54°
throat diameter	3.358 cm (1.393 inches)
throat area: 1 passage	53.94 cm^2 (8.360 in^2)
leading edge diameter	2.657 cm (1.046 inches)
trailing edge diameter	0.518 cm (0.204 inches)
Flow parameter	**Value**
Inlet Re_{C_x}	$0.977 \pm 0.028 \times 10^6$
Exit Re_{C_x}	$1.843 \pm 0.060 \times 10^6$
Inlet M_{IS}	0.383 ± 0.0006
Exit M_{IS}	1.321 ± 0.003
Inlet δ_f	3.2 cm (1.2 inch)
Inlet flow angle	63.6°
Design flow turning	136°

(all repeatabilities based on 95% confidence limits)

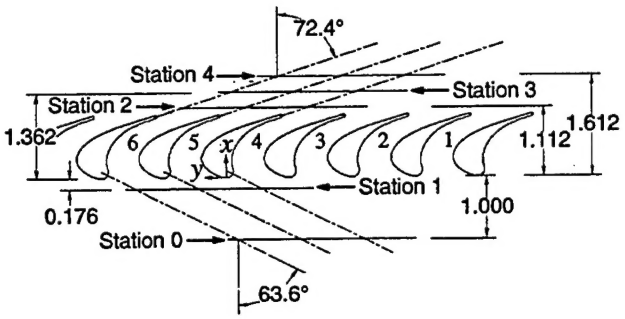

note: all distances nondimensionalized by axial chord, C_x

Fig. 2 Test section geometry and measurement plane locations

DESCRIPTION OF INSTRUMENTATION

Static Pressure Measurements Endwall surface static pressure data was obtained with an endwall instrumented with approximately 550 pressure taps. Pressure measurement taps were located in all passages. The test passage and two adjacent passages were instrumented with 87 pressure taps per passage. The taps extended axially from $x/C_x = -0.4$ to $x/C_x = 2.1$ and were arranged in 21 rows with either 4 or 5 taps per row. Decreasingly fewer taps were located in passages away from the test passage. The locations of the pressure taps in the three measurement passages will be shown in contour plots of endwall static pressure. Data from the three fully-instrumented passages was used to provide a periodicity check.

The two blades that formed Passage 5 were instrumented with static pressure taps to measure blade loading. The taps were located on 9 spanwise planes extending over the entire span of the blade. On both blades, pressure taps were located completely around the leading and trailing edge circles in order to verify periodicity. Also, spanwise symmetry was verified by comparing measurements on planes that were symmetric about midspan.

All pressures were measured with an electronically scanned strain gauge measurement system. The 100 kPa (15 psid) strain gauge transducers were typically calibrated every 20 minutes against a thermally isolated digiquartz calibration unit. Barometric pressure was used as the reference pressure. Rapid changes in the barometric pressure required more frequent calibrations. The repeatability of the pressure measurement system was 0.05%. This was determined by comparing the output of 26 transducers against a fixed mid-range pressure level.

The blade and endwall static pressure measurements were made with all measurement probes removed from the test section. To measure the inlet total pressure, two Kiel probes were located at the exit of the 8:1 upstream contraction (see Fig. 1), and one Kiel probe was located approximately 7 C_x upstream of the blades, but away from the measurement passages. These three probes agreed with each other to within system repeatability. To obtain the blade and endwall static pressure data, the pressure measurement system was programmed such that one reading represented 15 scans at a rate of 1 scan per second. Ten such readings were taken over approximately 10 minutes and were averaged.

Flow-Field Probe Measurements
Photographs and dimensions of the 3-hole boundary-layer probe and of the 5-hole pitch-yaw probe are shown in Fig. 3. The probes were 45° forward-facing pyramid probes and were nominally identical except for the measurement heads. Note that the probes were angled such that their measurement heads were located along the axis of the probe shaft. This was done so that when the probe was rotated, the location of the probe head would not change. The portion of the probe that retracted into the actuator had a circular cross-section of diameter 6.4 mm (0.25 in.). The primary portion of the probe exposed to the flow had a diamond cross-section of dimensions 3.6 mm × 6.4 mm (0.14 in. × 0.25 in.).

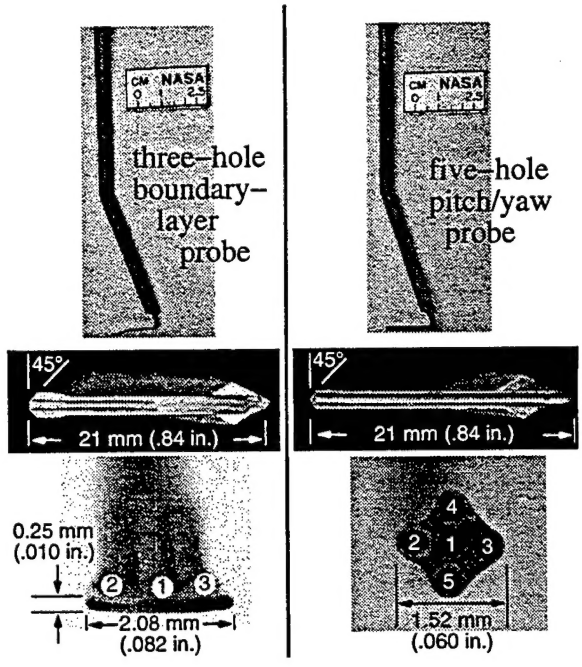

Fig. 3 Aerodynamic measurement probes

The reduction of data acquisition time was of primary concern in the facility. The time constants, τ, of the probes were measured to determine the wait time required when a probe was moved. The time constants were measured by applying a step change in pressure to the probes while they were connected to the transducers exactly as they were for the actual measurements. The time constants for the probes were: $\tau_{3-hole} = 0.82$ sec., and $\tau_{5-hole} = 0.55$ sec. The longer time constant of the 3-hole probe was caused by its smaller port openings. Wait times of five time constants were used to achieve greater than 99% recovery. Each probe port was measured with 3 separate transducers, and each port was scanned 5 times at a rate of 1 scan per second.

The probe was positioned by a remotely operated, computer controlled actuator. A flexible steel tape was used to bridge the gap formed by the pitchwise slot. A hole was drilled in the tape for the probe to pass through, and spring-loaded take-up reels on each end provided smooth operation. The step in the endwall caused by the pitchwise slot was less than 1 mm in height. The pitchwise extent of travel was shown in Fig. 2. Because the probe shaft was angled, the spanwise extent of travel was limited from $z = 0$ to $z = 0.54 \times$ span. The actuator system had the capability of automatically nulling the probe by adjusting the angle in order to drive $P_3 - P_2$ to zero. However, this capability was not used, since the time required to null the probe was much greater than five time constants. Rather than nulling the probes, a pitch-yaw calibration technique was used.

Another important feature of the probe actuator system was an electrical circuit that was used to detect the point at which the 3-hole boundary-layer probe touched the aluminum wall. Figure 3 shows a slight ($\approx 3°$) bend in the 3-hole probe at the measurement head tip. This bend allowed the tip to touch the wall first and flex slightly without damage. Touching the wall with the tip completed a circuit and stopped the actuator. This technique gave a reproducibility in the wall location of approximately ± 0.08 mm (± 0.003 in.). When the 3-hole probe touched the wall, the measurement location was taken as half the probe thickness. This gave a location of 0.13 mm (0.005 in.) from the endwall. In order to allow the touch circuit to work, the probe was electrically isolated from the actuator using heat-shrinkable tubing.

PROBE CALIBRATION TECHNIQUE

The probes were calibrated in a subsonic, free-jet facility and in the exits of enclosed, supersonic, converging-diverging nozzles. The following pressure coefficients were defined, generally following the work of Reichert and Wendt (1994) and of Dominy and Hodson (1993):

pitch angle:	$C_{p,\alpha} = (P_2 - P_3)/(P_1 - P_o)$
yaw angle:	$C_{p,\beta} = (P_5 - P_4)/(P_1 - P_o)$
total pressure:	$C_{p,1} = (P' - P_1)/(P_1 - P_o)$
static pressure:	$C_{p,o} = (P_o - P)/(P_1 - P_o)$
Mach number:	$C_{p,M} = P_o/P_1$

P_o is the average pressure of the outer probe ports, i.e., $P_o = (P_2 + P_3 + P_4 + P_5)/4$ for the 5-hole probe, and $P_o = (P_2 + P_3)/2$ for the 3-hole probe.

The calibration procedures for the 5-hole and the 3-hole probes were similar. The yaw angle, β, and its corresponding coefficients did not enter into the calibration of the 3-hole probe. In the calibration facility, the total and static pressures, P' and P, were measured along with the probe pressures P_1 through P_5. These measurements were made as the probe was traversed over a range of angles in increments of 5°. The traverse range was $\pm 25°$ in α, and $\pm 20°$ in β.

The first step in the calibration procedure was the determination of coefficient dependencies on flow angles. The average outer port pressure, P_o, was first calculated in order to calculate the pressure coefficients $C_{p,\alpha}$ and $C_{p,\beta}$. A least-squares regression was performed in order to fit the flow angles α and β, to fourth-order polynomials of $C_{p,\alpha}$ and $C_{p,\beta}$. Probe calibration symmetry was not assumed, so 15 unknown coefficients needed to be determined for each calibrated quantity. The regression coefficients were estimated by solving the least-squares system of equations. A sample of some input calibration data and the corresponding output calibration functions are shown graphically in Fig. 4.

A similar procedure was undertaken to calibrate for total and static pressures. The pressure coefficients $C_{p,1}$ and $C_{p,o}$ were fit as fourth-order polynomials in α and β. For the blade row surveys, the probe measurements were used to calculate $C_{p,\alpha}$ and $C_{p,\beta}$. The local flow angles, α and β were then determined from their calibration regressions. The two flow angles were then used to determine $C_{p,1}$ and $C_{p,o}$. With these values known, the local total and static pressures were easily determined from their definitions.

Relatively large uncertainties were related to the static pressure coefficient, $C_{p,o}$, and its calibration, so flow field static pressure measurements were the least reliable and will not be presented here. Some sample input calibration data and the corresponding output calibration functions for total pressure are shown graph-

ically in Fig. 5. The effects on total pressure of the bow shock in front of the probe were small because of the relatively low supersonic Mach numbers involved with these measurements, but a normal shock correction was still made. Probe calibrations were performed at Mach numbers ranging from 0.2 to 1.6. The pressure coefficient $C_{p,M}$, determined only from probe pressure port measurements, when corrected for flow angle, was found to correlate well with Mach number. Thus, a reasonable estimate of the Mach number was determined from $C_{p,M}$, α, and β. A normal shock correction could therefore be made for measurements with $M > 1.0$.

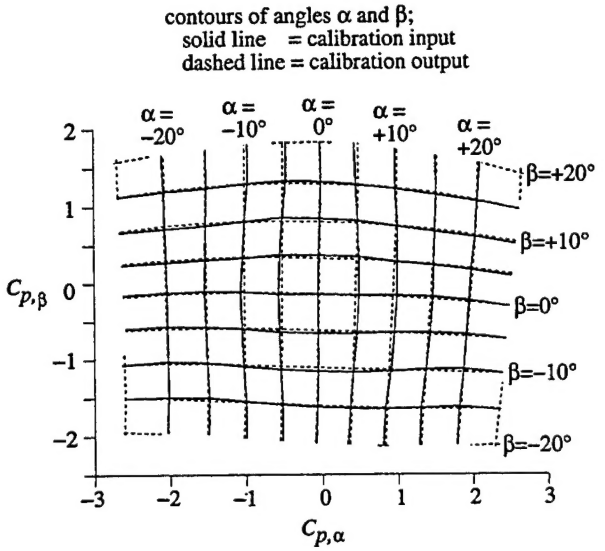

Fig. 4 Sample five-hole probe flow angle calibrations

Readings from a 5-hole probe will be biased near walls because the large gradient in P' across the endwall boundary layer is misinterpreted by the probe as a yaw angle in the flow, thus precluding use of the 5-hole probe near walls. Three-hole probe calibration data was obtained at several yaw angles to determine the range over which the total pressure and α calibrations were insensitive to β. The calibration data showed that the geometry of the 3-hole probe caused its total pressure and α calibrations to be independent of the yaw angle, β, for $-5° \leq \beta \leq +15°$, but dependent on β outside this range. Five-hole probe flow field measurements showed that local yaw angles could be less than $-5°$ at distances of $z/s \leq 0.04$ away from the endwall. Therefore, the use of the 3-hole probe is legitimate only in this near-endwall region.

Probe calibrations were verified in the cascade by turning the probe at different angles to the flow while maintaining the same spatial location. Deviations in measured flow angles for both α and β were less than 0.5°. Measured total pressure variations were less than 1.5% of the inlet dynamic pressure. Overall, the estimated uncertainty in flow angle measurements was $\pm 1.5°$, while the estimated uncertainty in total pressure coefficient was $\pm 1.7\%$ at the upstream, subsonic measurement planes and $\pm 2.1\%$ at the downstream, supersonic measurement planes.

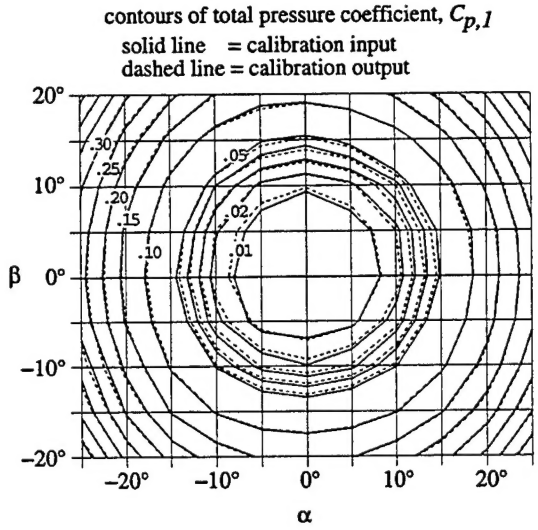

Fig. 5 Sample five-hole probe total pressure calibration

MEASUREMENT RESULTS

Static Pressure Measurements Figure 6 shows endwall static pressure distributions at high and low Reynolds numbers and at sonic and supersonic exit Mach numbers. The locations of the pressure taps appear in the figure along with the contours. As mentioned earlier, the figure shows the strong three-dimensionality of the flow – particularly evidenced by the fact that the $P/P'_{in} = 0.8$ contour line has a peak near mid-passage that is caused by the horseshoe/passage vortex. Also to be noticed from the figure is that the Reynolds number has almost no effect on the pressure distribution, and that the exit Mach number affects only the portion of the endwall downstream of the blade throat. Both of these features were to be expected. Figure 6 also provides evidence of the excellent flow periodicity.

Figure 7 shows blade pressure loading distributions at the same four cases. Also included in the figure are results of calculations with the three-dimensional Navier-Stokes CFD code of Chima (see Chima and Yokota, 1990). The results of the calculations are shown as lines in the figure, while the experimental data is shown as discrete points. The data shows excellent spanwise symmetry as evidenced by data on symmetric planes (e.g., 10% span and 90% span) typically overlaying each other. Again, note the strong flow three-dimensionality as evidenced by the spanwise variations in loading between $0.1\,C_x$ and $0.6\,C_x$ on the suction surface. Another interesting, but more subtle feature to note is that the lowest suction surface pressures between $0.90\,C_x$ and $0.95\,C_x$ occur at 25% and 75% of span. This feature is most obvious for the sonic exit cases (b. and d. in Fig. 7) but is also true for the supersonic exit cases. Flow field probe measurements to be presented in the next section will show that the horseshoe/passage vortex exits the trailing edge region at near 25% span causing this loading characteristic.

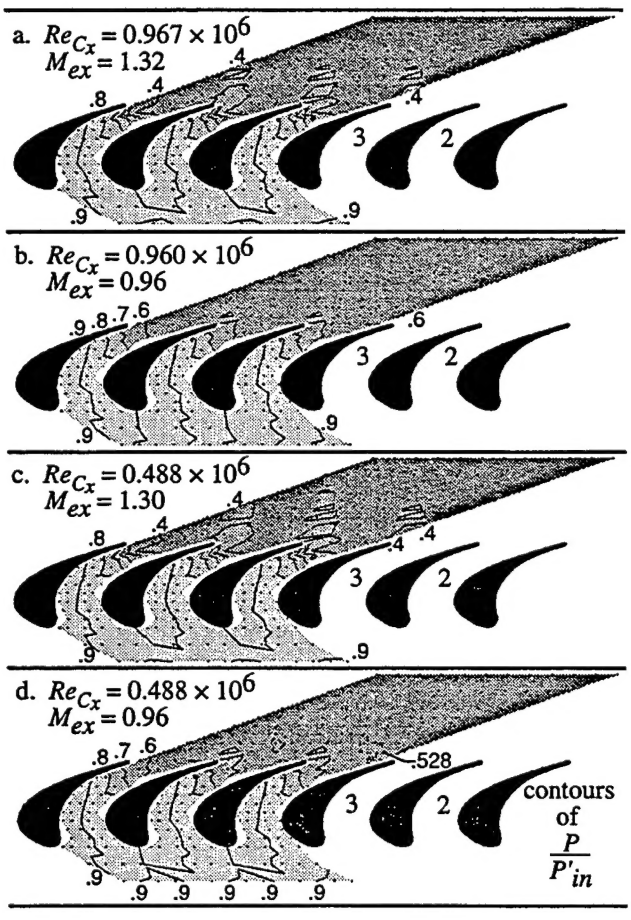

Fig. 6 Endwall static pressure distributions

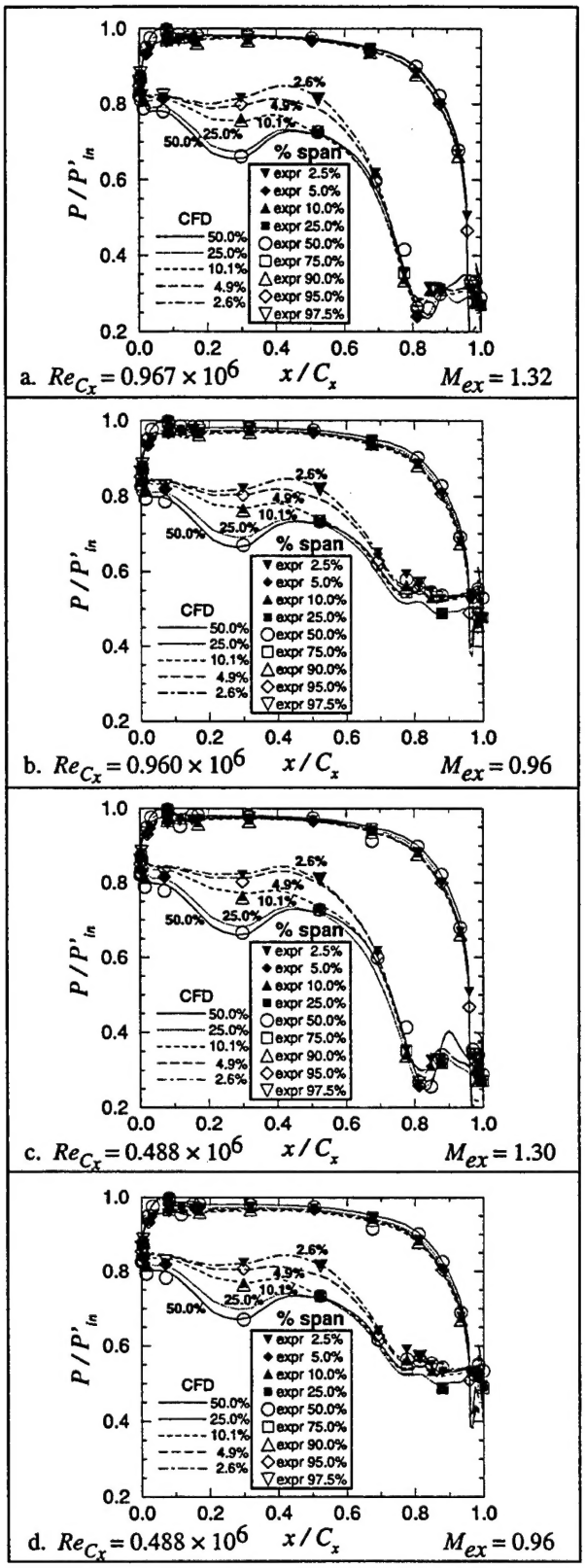

Fig. 7 Blade pressure loading distributions

Flow-Field Probe Measurements Flow field probe measurements include the pitch angle, α, the yaw angle, β, and the total pressure coefficient, $C_{p,t}$. The total pressure coefficient is defined as:

$$C_{p,t} = (P'_{in} - P')/(P'_{in} - P_{in})$$

Unlike the blade and endwall static pressure measurements, all of the flow field data presented here was obtained at $Re_{C_x} = 1.0 \times 10^6$ and at $M_{ex} = 1.3$. The data will first be presented as contour plots to show the three-dimensional features of the flow. The pitchwise integrated averages of the flow data will then be presented.

The flow field data are first given as contour plots viewed from upstream looking downstream. Figure 2 shows the axial locations and pitchwise extent of the five measurement planes. For all of the flow field data, measurements are presented using a combination of 3-hole and 5-hole probe data. Results from the 3-hole boundary-layer probe were used in the near-wall region, $z/s \leq 0.04$. In this region, there were 14 spanwise data points in each of 29 pitchwise survey locations. In the region $0.04 < z/s \leq 0.54$, 5-hole probe data were used. In this region, there were 62 pitchwise data points in each of 13 spanwise survey locations. The flow field data is shown in Figs. 8, 9, and 10. In general, the data show good agreement between the two probe results at $z/s = 0.04$.

Total pressure data for the five measurement planes is shown in Fig. 8. The data from the upstream planes shows the thick but uniformly periodic inlet boundary layer. Note that because of the large blunt leading edges of the blades, some effects of the blades can be seen, even one C_x upstream of the blade leading edge plane. Recall that the minimum blade surface pressure region at quarter span near the trailing edge shown in Fig. 7 was said to be the result of the horseshoe/passage vortex. The measurements at $x/C_x = 1.112$ (Station 2), just downstream of the trailing edge, clearly show the horseshoe/passage vortices exiting the blade row near each of the blade suction surfaces at one quarter of the full span. The nearly complete lack of any endwall boundary layer here also indicates that the inlet boundary layer low-momentum fluid is either being carried downstream by these vortices or has been convected to the suction surface by the passage vortex. Even this close to the trailing edge, the data shows that the wakes are distorted by the vortices. Further downstream, this distortion makes the wakes almost unrecognizable. At Station 2, very near the endwall and directly under the vortex loss cores ($y/s \approx 0.0$, $-.75$, and -1.5), are high gradient regions of $C_{p,t}$. The passage vortices are pulling in low-loss fluid of $C_{p,t} \approx 0.25$ from the freestream while also pulling in high-loss endwall boundary layer fluid of $C_{p,t} \approx 4.5$. It is interesting to note that even at the $x/C_x = 1.612$ location, the highest total pressure (lowest $C_{p,t} \approx 0.50$) is still very near the endwall, at less than $z/s = 0.05$. This high total pressure region is evident at y/s near -1.0 and -1.75. The strong three-dimensional effects are due somewhat to the thick inlet boundary layer but perhaps are due more to the high degree of flow turning.

In general, the total pressure data shows good periodicity and good spanwise symmetry. The Station 2 data suggests that a somewhat two-dimensional region near midspan exists after exiting the blade row. The Station 3 and 4 data however, while still showing good spanwise symmetry, show no significant regions near midspan with zero spanwise gradients. This implies that the upper- and lower-half flow structures are directly impacting each other.

Measurements of pitch angle, α, are shown in Fig. 9. These measurements show that the flow was quite uniform at $x/C_x = -1.000$ while also showing that the flow followed the prescribed inlet flow angle to within 0.4°. The pitchwise and spanwise average flow angle was within 0.2° of the nominal inlet flow angle of 63.6°. The data from Stations 1 through 4 show, in general, large variations in flow angle, particularly very close to the endwall. If the measurement of α exceeded the calibration range, the probe was approximately nulled before obtaining data. The data at the $x/C_x = -0.176$ plane show the strong influence of the blades on the flow. For each downstream plane contour plot, there is a dashed-line contour labeled 72° corresponding to the blade trailing edge metal angle. Contours with values greater than this angle indicate regions where the flow was overturned relative to the blade. Close to the trailing edge, $x/C_x = 1.112$, overturning predominates near the endwall as driven by the passage vortex secondary flow. The vortex drives flow underturning in the area above quarter span. Further downstream, the magnitude of overturning decreases. At the furthest downstream location, $x/C_x = 1.612$, there is some underturning at midspan.

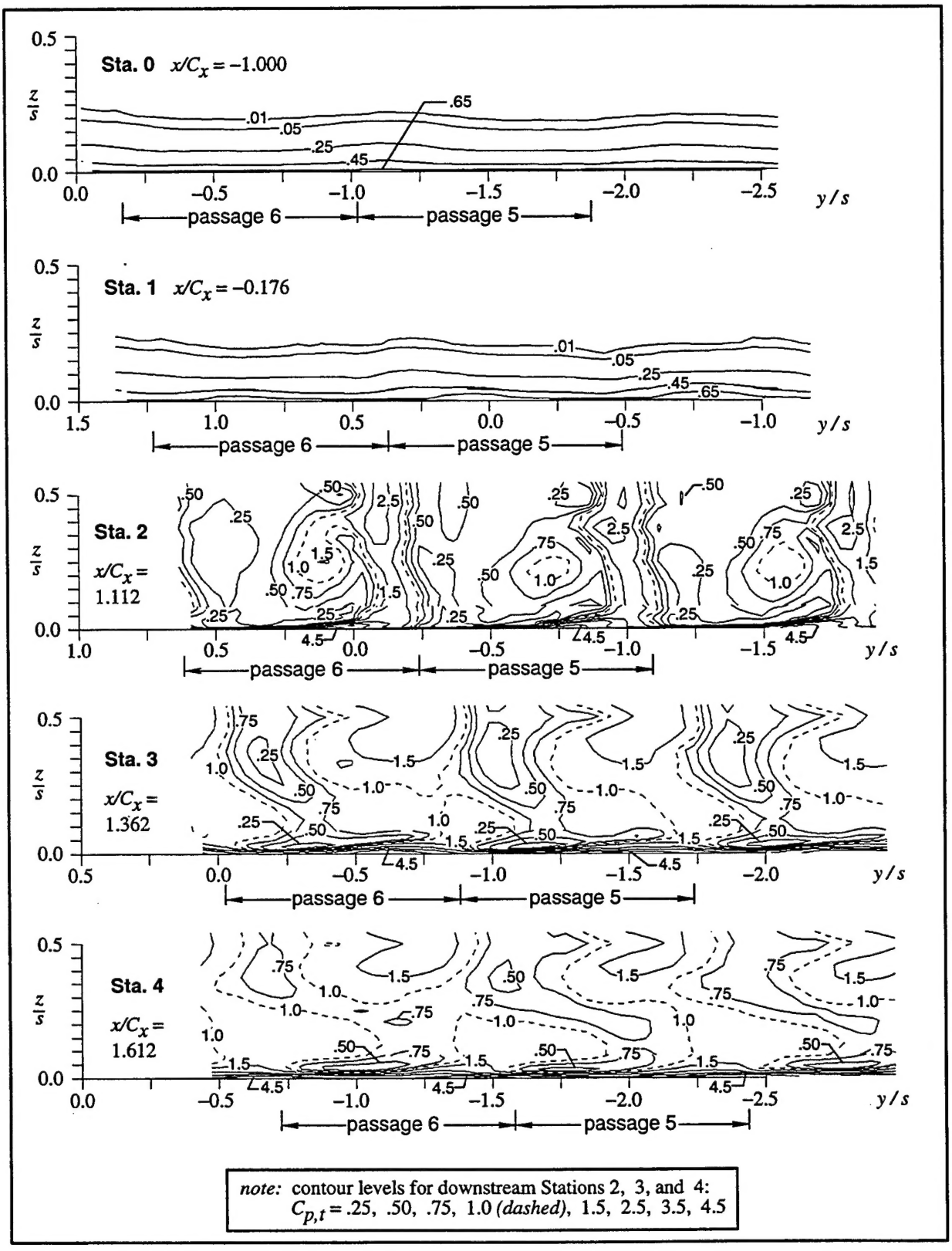

Fig. 8 Total pressure coefficient measurements

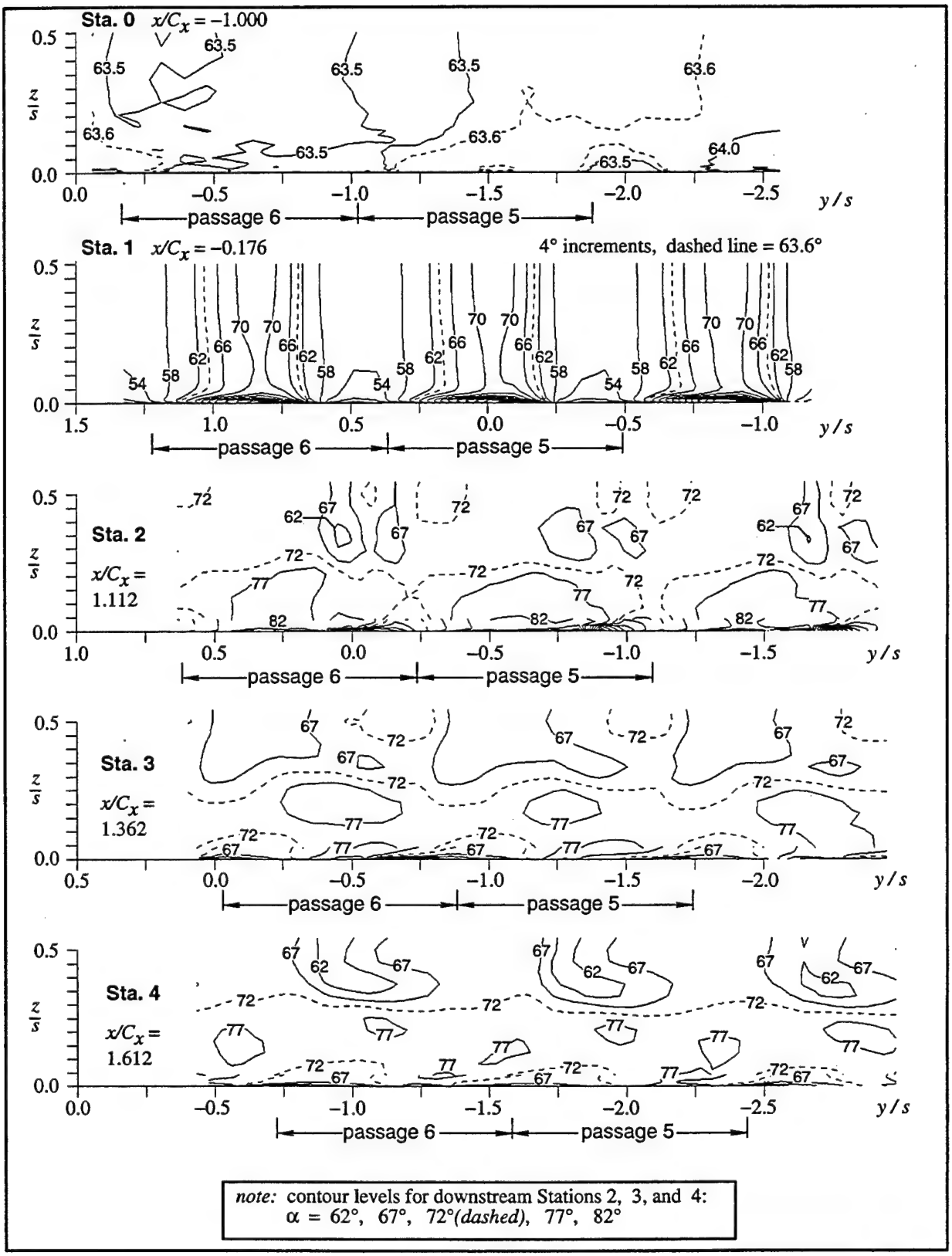

Fig. 9 Pitch angle α measurements

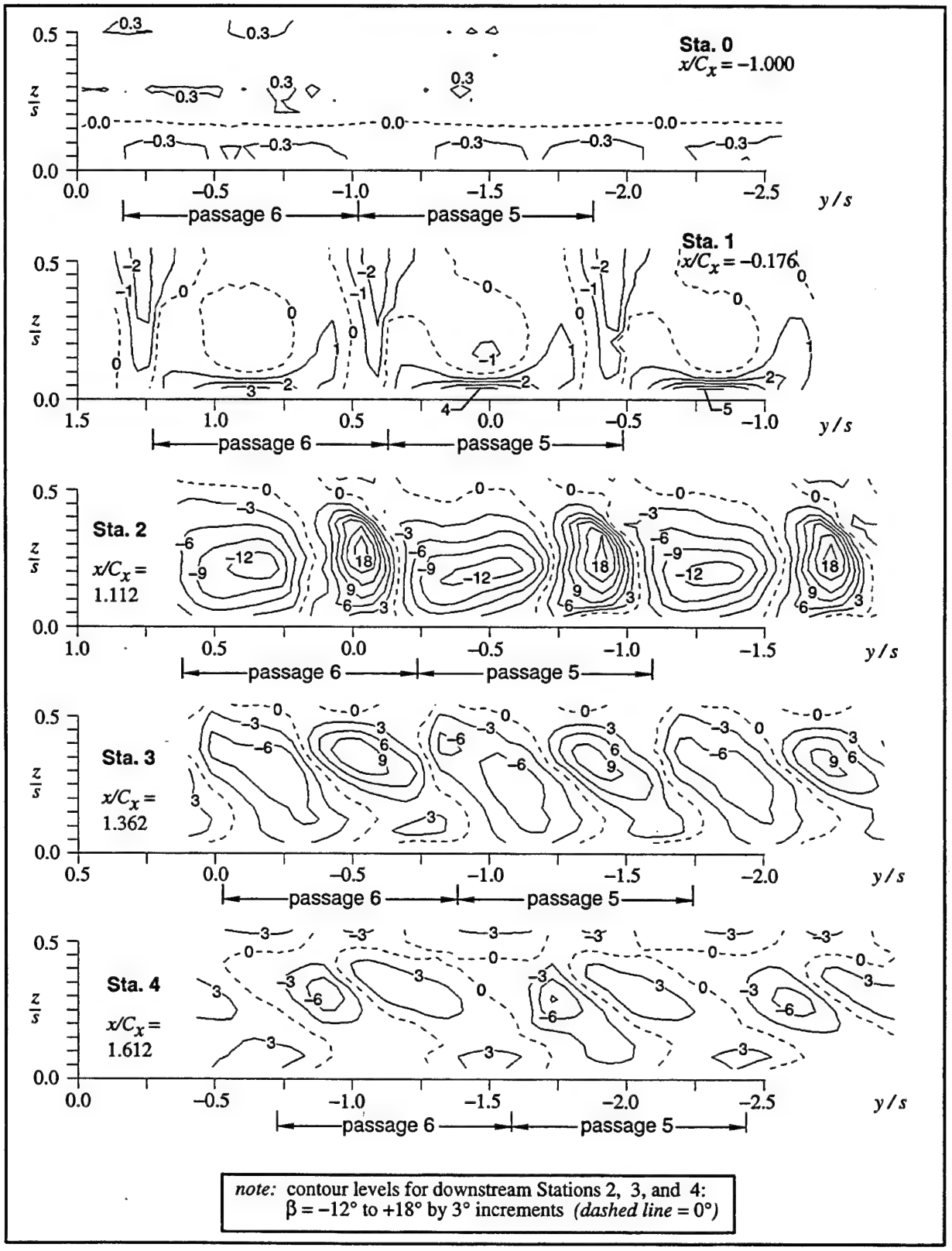

Fig. 10 Yaw angle β measurements

The locations of the vortices that were evident in the $C_{p,t}$ contours in Fig. 8 are also indicated in the contour plots of α. However, it should be noted that in general, the vortex loss core is not coincident with the kinematic vortex core. The local pitch angle is greater than the mean flow angle on one side of the vortex, and less on the other side. At the $x/C_x = 1.112$ plane, α is approximately 72° across all three passages at $z/s = 0.25$. Large gradients in α are seen at y/s near 0.10 in Passage 6, y/s near -0.75 in Passage 5, and y/s near -1.60 in Passage 4. Peak-to-peak differences in α across these gradients are on the order of 15 to 20 degrees. At the $x/C_x = 1.362$ and 1.612 planes, α is approximately 72° across all three passages at $z/s = 0.30$, indicating that the vortices have risen slightly off of the endwall.

Measurements of yaw angle, β are shown in Fig. 10. Again, the measurements show very uniform flow one C_x upstream of the blade leading edge plane, and show strong blade effects at $x/C_x = -0.176$. The β measurements at the $x/C_x = -0.176$ plane show some evidence of spanwise asymmetry. Near midspan β reaches $-2°$ which is slightly outside of its uncertainty range. This error may be caused by the probe interfering with the horseshoe vortex upstream of the blade leading edge. Endwall heat transfer measurements in the same facility (Giel et al., 1996) showed that because of the large, blunt leading edge, the horseshoe vortex clearly affects the flow at $x/C_x = -0.176$. The fact that the probe was angled back into the downstream region would also tend to accentuate any interference.

The locations of the vortex cores at $x/C_x = 1.112$ are more evident for these β measurements than they were for the α measurements. The cores were centered at the point where $\beta = 0°$, between the maximum value of $\beta = +18°$ and the minimum value of $-12°$, near the same spanwise and pitchwise locations noted above. Further downstream, the flow begins to straighten, but the vortex core locations remain evident. The data suggests that the vortex cores had risen from about $z/s = 0.22$ at $x/C_x = 1.112$ to about $z/s = 0.32$ at $x/C_x = 1.362$ and 1.612, reasonably consistent with the α measurements.

Area-weighted, pitchwise integrated averages were calculated for all of the measured quantities over Passages 5 and 6 at the five measurement planes. These averages are shown in Figs. 11, 12, and 13 as a function of span. As in the contour plots described above, the near-wall data in the figures was obtained with the 3-hole boundary-layer probe while the remainder was obtained with the 5-hole pitch/yaw probe. Some discrepancies between the 3-hole and 5-hole probe data are seen in the α averages of Fig. 12. Note though, that all of the discrepancies are within the experimental uncertainty. Besides measurement uncertainty, part of the reason for the discrepancies may be that spanwise 3-hole probe surveys were taken at only half the pitchwise resolution of the 5-hole probe data. Therefore, some flow features with large gradients such as wakes may not have been sufficiently resolved, particularly at Station 2, thus affecting the integrations.

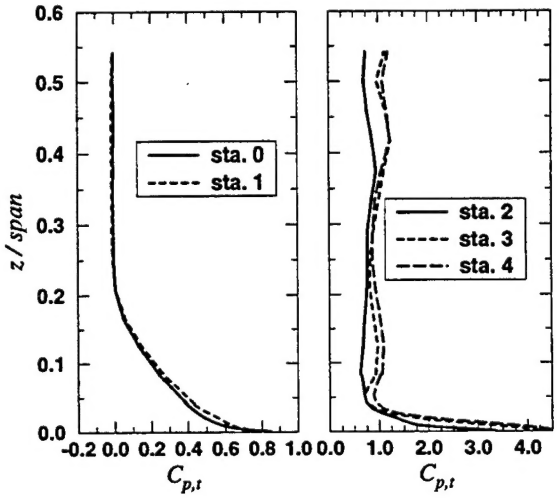

Fig. 11 Pitchwise averaged total pressure coefficient

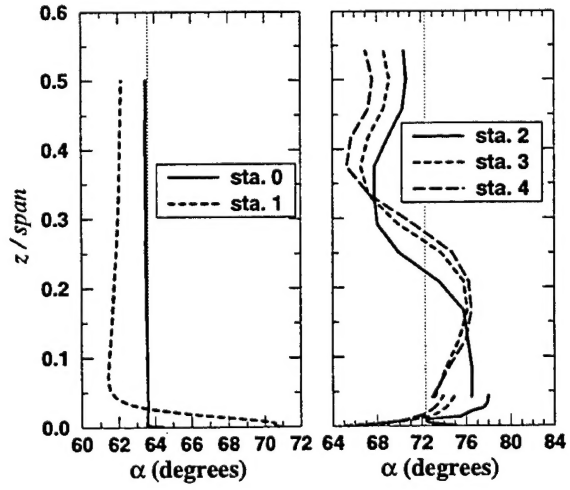

Fig. 12 Pitchwise averaged pitch angle α

The thick inlet boundary layer is clearly seen in Fig. 11 at Stations 0 and 1. Downstream of the blade row a significantly thinner endwall boundary layer is seen, but the near-wall measurements also show its

streamwise growth. The passage vortices and their associated loss cores are not evident in the downstream averages although a weak minimum does appear between $z/s \approx 0.1$ and midspan. This is because the wake losses are dominant at $x/C_x = 1.112$, and Fig. 8 showed that the vortex and wake losses are reasonably mixed out at the further downstream planes.

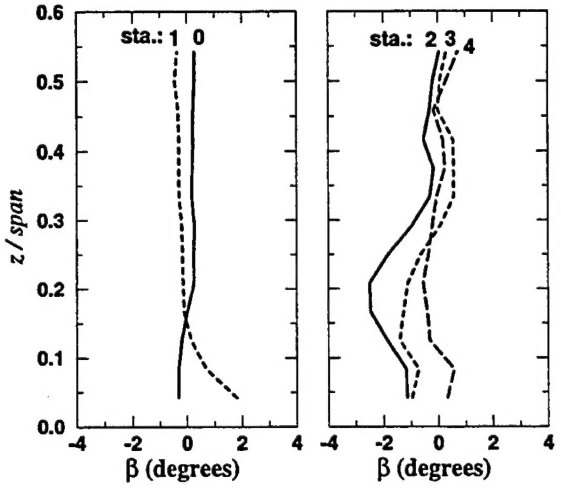

Fig. 13 Pitchwise averaged yaw angle β

Pitchwise averaged flow angle α measurements are shown in Fig. 12. The Station 1 data again shows the significant influence of the blades on the flow at $x/C_x = -0.176$ The effects of the passage vortices are clearly seen in the downstream averages. As noted in the discussion of Fig. 9, the vortices rise towards midspan as the flow proceeds downstream. As expected, the Station 2 near-wall data shows complex but always overturned flow. Stations 3 and 4, however, show underturning in a thin region near the endwall.

Despite large local values of flow angle β as shown in Fig. 10, Fig. 13 shows that the pitchwise averaged β angle is within approximately $\pm 2°$, even at the downstream measurement planes. Since the differences between measurement stations in the pitchwise averaged values of β are not significantly outside the experimental uncertainty, no conclusions can be drawn based on the spanwise variations shown in Fig. 13.

SUMMARY AND CONCLUSIONS

The measurements made in this facility showed that very good periodicity existed for the test passage and its adjacent passages. Achieving periodicity is especially important for data that is intended for verification of CFD analyses, since this is an assumption of many Navier-Stokes analyses. The measurements at the cascade inlet also show a well-defined and pitchwise uniform flow that is highly desirable for comparing with CFD analyses.

The data presented in this work show highly complex three-dimensional flow structures, which were measured with a high degree of spatial resolution. The strong horseshoe/passage vortex system was seen to be largely responsible for the three-dimensionality. The vortices are due in part to the thick inlet boundary layer, but perhaps more so to the high degree of flow turning. Their impact on the wake and the entire downstream flow field needs to be understood and modeled more accurately as the current trend towards higher turning turbine airfoils continues. The aerodynamic data presented here, along with the endwall heat transfer data presented by Giel et al. (1996) comprise a complete set of data suitable for CFD code and model validation. Electronic tabulations of the data are available at each measurement location. Measurements of the blade and endwall surface pressures are also available. The tabulated flow field results are given at their individual spatial locations and as integrated pitchwise averages. Overall performance, as determined from flow field averages, is important from a design standpoint and is often the primary objective in CFD predictions. For CFD verification, however, it is often more appropriate to compare measurements and analytic results at discrete points rather than comparing them on an overall basis. These pointwise comparisons have the potential of giving the insight needed to improve the predictive capability of CFD codes and models.

ACKNOWLEDGEMENTS

This work was supported by the NASA Lewis Research Center under contract NAS3-27186 with NYMA, Inc., with Mr. Robert J. Boyle as monitor. The authors also would like to acknowledge the assistance of Mr. Jose Gonsalez and Dr. Warren Hingst in calibrating the aerodynamic probes.

REFERENCES

Chima, R. V., and Yokota, J. W., 1990, "Numerical Analysis of Three-Dimensional Viscous Internal Flows," AIAA *Journal*, Vol. 28, No. 5, pp. 798-806.

Dominy, R. G., and Hodson, H. P., 1993, "An Investigation of Factors Influencing the Calibration of Five-Hole Probes for Three-Dimensional Flow Measurements," ASME *Journal of Turbomachinery*, Vol. 115, pp. 513-519.

Giel, P. W., Sirbaugh, J. R., Lopez, I., and VanFossen, G. J., 1994, "Three-Dimensional Navier-Stokes Analysis and Redesign of an Imbedded Bellmouth Nozzle in a Turbine Cascade Inlet Section," ASME paper 94-GT-237, and accepted for publication in the ASME *Journal of Turbomachinery*.

Giel, P. W., Thurman, D. R., VanFossen, G. J., Hippensteele, S. A., and Boyle, R. J., 1996, "Endwall Heat Transfer Measurements in a Transonic Turbine Cascade," to be presented at the ASME International Gas Turbine Conference, Birmingham, England, June 10-13.

Gregory-Smith, D. G., Graves, C. P., and Walsh, J. A., 1988, "Growth of Secondary Losses and Vorticity in an Axial Turbine Cascade," ASME *Journal of Turbomachinery*, Vol. 110, No. 1, pp. 1-8.

Gregory-Smith, D. G., and Graves, C. P., 1983, "Secondary Flows and Losses in a Turbine Cascade," in: *Viscous Effects in Turbomachines*, AGARD-CP-351.

Graham, C. G., and Kost, F. H., 1979, "Shock Boundary Layer Interaction on High Turning Transonic Turbine Cascades," ASME paper 79-GT-37.

Kiock, R., Lehthaus, F., Baines, N. C., and Sieverding, C. H., 1986, "The Transonic Flow Through a Plane Turbine Cascade as Measured in Four European Wind Tunnels," ASME *J. of Engr. for Gas Turbines and Power*, Vol. 108, pp. 277-284.

Langston, L. S., Nice, M. L., and Hooper, R. M., 1977, "Three Dimensional Flow Within a Turbine Cascade Passage," ASME *Journal of Engineering for Power*, Vol. 99, No. 1, pp. 21-28.

Marchal, P., and Sieverding, C. H., 1977, "Secondary Flows Within Turbomachinery Bladings," in: *Secondary Flows Within Turbomachines*, AGARD-CP-214.

Mee, D. J., Baines, N. C., Oldfield, M. L. G., and Dickens, T. E., 1992a, "An Examination of the Contributions to Loss on a Transonic Turbine Blade in Cascade," ASME *Journal of Turbomachinery*, Vol. 114, No. 1, pp. 155-162.

Mee, D. J., Baines, N. C., and Oldfield, M. L. G., 1992b, "Detailed Boyndary Layer Measurements on a Transonic Turbine Cascade," ASME *Journal of Turbomachinery*, Vol. 114, No. 1, pp. 163-172.

Moustapha, S. H., Paron, G. J., and Wade, J. H. T., 1985, "Secondary Flow in Cascades of Highly Loaded Turbine Blades," ASME paper 85-GT-135.

Reichert, B. A., and Wendt, B. J., 1994, "A New Algorithm for Five-Hole Probe Calibration, Data Reduction, and Uncertainty Analysis," NASA TM-106458.

Verhoff, V. G., Camperchioli, W. P., and Lopez, I., 1992, "Transonic Turbine Blade Cascade Testing Facility," AIAA Paper No. 92-4034, NASA TM-105646.

Yamamoto, A., 1987a, "Prediction and Development of Secondary Flows and Losses in Two Types of Straight Turbine Cascades: Part 1 - A Stator Case," ASME *Journal of Turbomachinery*, Vol. 109, No. 2, pp. 186-193.

Yamamoto, A., 1987b, "Prediction and Development of Secondary Flows and Losses in Two Types of Straight Turbine Cascades: Part 2 - A Rotor Case," ASME *Journal of Turbomachinery*, Vol. 109, No. 2, pp. 194-200.

REPORT DOCUMENTATION PAGE

Form Approved
OMB No. 0704-0188

1. AGENCY USE ONLY (*Leave blank*)	2. REPORT DATE	3. REPORT TYPE AND DATES COVERED
	December 1996	Technical Memorandum

4. TITLE AND SUBTITLE

Three-Dimensional Flow Field Measurements in a Transonic Turbine Cascade

5. FUNDING NUMBERS

WU–523–26–13

6. AUTHOR(S)

P.W. Giel, D.R. Thurman, I. Lopez, R.J. Boyle, G.J. Van Fossen, T.A. Jett, W.P. Camperchioli, and H. La

7. PERFORMING ORGANIZATION NAME(S) AND ADDRESS(ES)

NASA Lewis Research Center
Cleveland, Ohio 44135–3191
and
U.S. Army Research Laboratory
Cleveland, Ohio 44135–3191

8. PERFORMING ORGANIZATION REPORT NUMBER

E–10584

9. SPONSORING/MONITORING AGENCY NAME(S) AND ADDRESS(ES)

National Aeronautics and Space Administration
Washington, DC 20546–0001
and
U.S. Army Research Laboratory
Adelphi, Maryland 20783–1145

10. SPONSORING/MONITORING AGENCY REPORT NUMBER

NASA TM–107388
ARL–TR–1252

11. SUPPLEMENTARY NOTES

Prepared for the 41st Gas Turbine and Aeroengine Congress sponsored by the International Gas Turbine Institute of the American Society of Mechanical Engineers, Birmingham, United Kingdom, June 10–13, 1996. P.W. Giel, NYMA, Inc., 2001 Aerospace Parkway, Brook Park, Ohio 44142 (work funded under NASA Contract NAS3–27186); D.R. Thurman and I. Lopez, U.S. Army Research Laboratory, NASA Lewis Research Center; R.J. Boyle, G.J. Van Fossen, T.A. Jett, W.P. Camperchioli, and H. La , NASA Lewis Research Center. Responsible person, Robert J. Boyle, organization code 5820, (216) 433–5889.

12a. DISTRIBUTION/AVAILABILITY STATEMENT

Unclassified - Unlimited
Subject Categories 02 and 07

This publication is available from the NASA Center for AeroSpace Information, (301) 621–0390.

12b. DISTRIBUTION CODE

13. ABSTRACT (*Maximum 200 words*)

Three-dimensional flow field measurements are presented for a large scale transonic turbine blade cascade. Flow field total pressures and pitch and yaw flow angles were measured at an inlet Reynolds number of 1.0×10^6 and at an isentropic exit Mach number of 1.3 in a low turbulence environment. Flow field data was obtained on five pitchwise/spanwise measurement planes, two upstream and three downstream of the cascade, each covering three blade pitches. Three-hole boundary layer probes and five-hole pitch/yaw probes were used to obtain data at over 1200 locations in each of the measurement planes. Blade and endwall static pressures were also measured at an inlet Reynolds number of 0.5×10^6 and at an isentropic exit Mach number of 1.0. Tests were conducted in a linear cascade at the NASA Lewis Transonic Turbine Blade Cascade Facility. The test article was a turbine rotor with 136° of turning and an axial chord of 12.7 cm. The flow field in the cascade is highly three-dimensional as a result of thick boundary layers at the test section inlet and because of the high degree of flow turning. The large scale allowed for very detailed measurements of both flow field and surface phenomena. The intent of the work is to provide benchmark quality data for CFD code and model verification.

14. SUBJECT TERMS

Gas turbines; Flow measurement; Cascade wind tunnel; Transonic flow; Supersonic turbines

15. NUMBER OF PAGES

16

16. PRICE CODE

A03

17. SECURITY CLASSIFICATION OF REPORT	18. SECURITY CLASSIFICATION OF THIS PAGE	19. SECURITY CLASSIFICATION OF ABSTRACT	20. LIMITATION OF ABSTRACT
Unclassified	Unclassified	Unclassified	